

Displacement-Based Fragility Curves for Seismic Assessment of Adobe Buildings in Cusco, Peru.

Nicola Tarque,^{a)} Helen Crowley,^{b)} M.EERI, Rui Pinho,^{c)} M.EERI, and Humberto Varum^{d)}

The seismic vulnerability of single-story adobe dwellings located in Cusco, Peru, is studied based on a mechanics-based procedure, which considers the analysis of in-plane and out-of-plane failure mechanisms of walls. The capacity of each dwelling is expressed as a function of its displacement capacity and period of vibration and is evaluated for different limit states to damage. The seismic demand has been obtained from several displacement response spectral shapes. From the comparison of the capacity with the demand, probabilities of failure have been obtained for different PGA values. The results indicate that fragility curves in terms of PGA are strongly influenced by the response spectrum shape; however, this is not the case for the derivation of fragility curves in terms of limit state spectral displacement. Finally, fragility curves for dwellings located in Pisco, Peru, were computed and the probabilities of failure were compared with the data obtained from the 2007 Peruvian earthquake.

INTRODUCTION

The collapse of adobe buildings due to earthquakes has caused considerable loss of life in third world countries. However, earth is generally the least expensive construction material and in many cases the only one available to the population in rural areas around the world (Bariola and Sozen 1990). The high seismic vulnerability of earthen buildings is due to an undesirable combination of the mechanical properties of dry earth: (1) earthen structures are

^{a)} ROSE School, IUSS Pavia, Via Ferrata 1, 27100 Pavia, Italy.

Division of Civil Engineering, Catholic University of Peru, Av. Universitaria 1801, Lima 32, Peru.

^{b)} European Centre for Training and Research in Earthquake Engineering, EUCENTRE, 27100 Pavia, Italy.

^{c)} Department of Structural Mechanics, University of Pavia, Via Ferrata 1, 27100 Pavia, Italy.

^{d)} Department of Civil Engineering, University of Aveiro, 3810-193, Aveiro, Portugal.

massive and thus attract large inertial forces, (2) they are weak and cannot resist these forces, and (3) they are brittle and break without warning (Blondet et al. 2006).

In this research, a mechanics-based procedure, which is based on the concepts of displacement-based design/assessment, has been applied to assess the seismic vulnerability of existing single-story adobe dwellings within a probabilistic framework. Different limit states for in-plane and out-of-plane failure have been defined and the capacity of adobe walls has been estimated as a function of the failure mechanism. The displacement capacity formulae, the period-height relationship, and the limit state properties are presented herein as common to adobe buildings in general, whereas the seismic capacity for adobe dwellings in Cusco—a city located in the Peruvian highlands—and the seismic demand in that city have been computed as an application of the proposed methodology. Finally, the conditional seismic risk for adobe dwellings in this region has been analyzed through the generation of analytical fragility curves as a function of peak ground acceleration (PGA) and spectral displacement at the limit state period of vibration ($S_d(T_{Ls})$). Finally, the described methodology has been applied to another Peruvian city (Pisco) where, in 2007, an earthquake destroyed the majority of the adobe and unreinforced masonry buildings. The procedure presented herein can be applied to other adobe dwellings around the world in a similar manner by taking into account their specific geometric properties.

FRAGILITY CURVES FOR IN-PLANE AND OUT-OF-PLANE BEHAVIOR

Fragility curves have been derived for adobe dwellings herein using the displacement-based earthquake loss assessment (DBELA) methodology (e.g., Crowley et al. 2004). The main concept of DBELA is the comparison of the displacement capacity of the building stock and the imposed displacement demand from a given scenario earthquake. In this method, random populations of buildings are generated using Monte Carlo simulation, and the displacement capacity and period of vibration of each building at three different limit states is calculated using simple mechanics-based and empirical equations. The displacement demand to each building is calculated from a displacement response spectrum (considering the equivalent viscous damping at the limit state in question) at the effective limit state period of vibration. The probability of exceedance is obtained for the first limit state by calculating the ratio between the number of dwellings with a displacement capacity lower than the displacement demand and the total number of dwellings (Figure 1). The probability of

exceeding the following limit states is obtained from the ratio between the number of dwellings that exceeded the previous limit state and that still have a displacement capacity lower than the displacement demand at the subsequent limit state, and the total number of dwellings. This evaluation can be repeated for a number of displacement response spectra (DRS), each with increasing levels of intensity (in terms of PGA or spectral displacement at a given period, for example) and plotted to produce fragility curves.

CAPACITY OF ADOBE DWELLINGS

OUT-OF-PLANE RESPONSE

Adobe material is brittle; with just a small amount of movement the walls forming a corner of an adobe building can separate from each other with vertical cracks (Figure 2). Adobe buildings typically do not have vertical or horizontal confinement elements (such as beams or columns) that can form a rigid diaphragm with the roof. Hence, adobe walls will try to behave independently of each other. If corner connections do not completely fail, some cracks at the mid-height of the wall can be expected due to vertical bending. When the adobe walls subjected to out-of-plane loads are completely separated from the perpendicular walls, the only conditions controlling stability are rocking behavior and the slenderness of the wall (i.e., the ratio of height over thickness of the wall).

The displacement-based seismic analysis method for out-of-plane bending of unreinforced masonry (URM) walls developed by Doherty et al. (2002) and Griffith et al. (2003, 2005) has been applied to adobe buildings in the present study. This procedure is straightforward and is based on a linearized displacement-based approach adapted for a wide variety of URM wall boundary conditions (parapets and simply supported walls, as shown in Figure 3). The main goal of the method is to predict the response of URM walls when dynamically loaded, taking into account their reserve capacity due to rocking (Melis 2002). Readers are referred to Doherty et al. (2002) and Griffith et al. (2003, 2005) for further information of the methodology.

Limit States and Displacement Capacity

According to Doherty et al. (2002) the single-degree-of-freedom (SDOF) equivalent system of a cracked URM wall rocking with large horizontal displacements may be modeled as rigid blocks separated by fully cracked cross sections where the resultant inertia force is

applied at two-thirds of the height of a parapet wall and one-third of the upper half of the simply supported wall from its mid-point (Figure 4). This assumption leads to a bilinear curve to represent the force-displacement relationship of a URM wall (Figure 5).

However, the individual blocks of the URM wall can deform significantly when subjected to high precompression. In this case the nonlinear force-displacement of these walls can be idealized by means of a suitable trilinear curve defined by three displacement parameters, Δ_1 , Δ_2 , Δ_u , and the force parameter F_0 (Figure 5, Doherty et al. 2002, Griffith et al. 2003).

The displacement Δ_1 is related to the initial stiffness and Δ_2 is related to the secant stiffness K_2 ; Δ_u is the ultimate displacement (i.e., the point of static instability in the wall) and thus displacements greater than Δ_u mean that the wall will collapse; $F_0 = \lambda W$ is the force at incipient rocking (which results from a rigid body analysis) and is also called the “rigid threshold resistance”; λ is the collapse multiplier factor and is calculated based on collapse mechanisms (as described in the following sections), and W is the total weight of the wall. F is the lateral static strength and refers to the force-plateau of the real nonlinear curve and can be computed from F_0 .

From simple static equilibrium of the rigid parapets (Figure 3a and 4), the ultimate displacement, Δ_u , at the top of walls can be obtained as equal to the wall thickness, t . For adobe walls a steeper descending branch of the trilinear idealization is expected, and thus the ultimate displacement Δ_u will be affected by reduction factors, as explained later; however, it is noted that laboratory tests on adobe walls are recommended to reliably define such displacement limit state values.

The lateral static strength (F) and the ultimate displacement (Δ_u) are not affected by uncertainties in properties such as the elasticity modulus, but rather the geometry, boundary conditions, and applied vertical forces (Griffith et al. 2003). The displacements Δ_1 and Δ_2 can be related to material properties and the state of degradation of the mortar at the pivot points, and are given as a proportion of Δ_u (see Table 1), as proposed by Griffith et al. (2003). According to Doherty et al. (2002), the effective width of the mortar in the cracked bedjoint for walls classified as severely degraded was approximately 90% of the original width. Moderately degraded walls had effective bedjoint widths that were essentially equal to their original widths. The authors assume that due to the usual high degradation of adobe, the

effective width will be less than that of URM, and thus the ultimate displacement is reduced by a factor 0.8 ($\Delta_u = 0.8t$).

Table 1. Displacement ratios for the trilinear model (Griffith et al. 2003)

State of degradation at cracked joint	$\rho_1 = \Delta_1 / \Delta_u$ (%)	$\rho_2 = \Delta_2 / \Delta_u$ (%)
New	6	28
Moderate	13	40
Severe	20	50

Just one limit state has been defined for the out-of-plane behavior (Equation 1), which defines if the wall will collapse or not. The ultimate limit state, defined as LS_u , is related to the period of vibration evaluated with the secant stiffness (K_2).

$$LS_u = \phi \cdot \Delta_u = \phi(0.8t) \quad (1)$$

where t is the wall thickness and ϕ is a factor from 0.8 to 1 to take into account the degradation of existing masonry walls (Restrepo-Velez and Magenes 2004).

Period of Vibration

Once the out-of-plane displacement capacity has been calculated (Equation 1), the period of vibration is required in order to estimate the displacement demand. Following the work of Griffith et al. (2003), the lateral static strength, F , can be evaluated using Equation 2 and the secant stiffness, K_2 , by Equation 3, where $F_o = \lambda W$ is the force necessary to trigger overturning.

$$F = F_o \left(1 - \frac{\Delta_2}{\Delta_u} \right) = \lambda W \left(1 - \frac{\Delta_2}{\Delta_u} \right) \quad (2)$$

$$K_2 = \frac{F}{\Delta_2} = \frac{\lambda W}{\Delta_2} \left(1 - \frac{\Delta_2}{\Delta_u} \right) \quad (3)$$

The secant stiffness K_2 is used to evaluate the period of vibration at the ultimate limit state. This is because it has been found that the use of this stiffness is a reliable parameter for the determination of the displacement demand in the large amplitude displacement region (Griffith et al. 2003). The period of vibration for the ultimate limit state can be obtained from: $T = 2\pi(M/K_2)^{0.5}$ with the stiffness represented by Equation 3 and the total mass by W/g . Equation 5 is obtained by rewriting Equation 4 for the ultimate limit state, LS_u ($\Delta_{LSu} = \phi\Delta_u$), and substituting the ratio Δ_2/Δ_u with ρ_2 .

$$T_2 = 2\pi \sqrt{\frac{\Delta_u \cdot \Delta_2}{\lambda g(\Delta_u - \Delta_2)}} \quad (4)$$

$$T_{LSu} = 2\pi \sqrt{\frac{\Delta_{LSu} \cdot \rho_2}{\lambda \phi g(1 - \rho_2)}} \quad (5)$$

The capacity (displacement and period) of a URM wall is directly compared to the displacement spectrum considering 5% damping. The demand should be multiplied by 1.5 for this comparison since the displacements of the trilinear curve presented in this work refer to values measured at the top wall, which are 1.5 greater than the displacement of the SDOF system (Griffith et al. 2005).

Collapse Mechanisms (for the Evaluation of λ)

In the work done by D'Ayala and Speranza (2003), some typical and feasible collapse mechanisms for URM buildings have been defined (Figure 6). These mechanisms have been identified through post earthquake damage inspections.

According to the damage survey undertaken following the 2007 Pisco earthquake, the most typical failure mode for single-story adobe buildings was due to Collapse Mechanisms A, C, and D, as shown in Figure 6 (Blondet et al. 2008). It can be assumed that those mechanisms can be extended to dwellings in Cusco. There are other failure mechanisms typical of unreinforced masonry buildings, such as the U-shaped failure with the bottom of the U at about mid-height on the wall; however, for simplicity just Collapse Mechanisms A, C, and D are considered in this study.

D'Ayala and Speranza (2003) developed equations to calculate the associated failure load factor for each mechanism in Figure 6 (i.e., the collapse multiplier, $\lambda = F/W$, that is, the ratio between the maximum lateral force for static stability over the total weight of the wall). A modification of those equations based on experimental tests was applied by Restrepo-Velez (2004) and these modified equations have been used herein. For brevity, only the equation for Mechanism A is provided herein (see Equation 6 and Figure 7) and the reader is referred to Restrepo-Velez (2004) for full details of the other mechanisms.

$$\lambda = \frac{\frac{t^2 L}{2} + \beta \cdot \Omega_{pef} \frac{h_s}{3} \mu_s \cdot s \cdot b \frac{(r+1)}{2} + \frac{K_r L t}{2}}{h_s \left(\frac{tL}{2} + K_r L \right)} \quad (6)$$

where t and L are the thickness and length of the front walls, β is the number of edge and internal perpendicular walls, Ω_{pef} is a partial efficiency factor to account for the limited effect of friction (Equation 7), h_s is the height of the failing portion of the wall, μ_s is the friction coefficient, s is the staggering length (normally half the brick length), b is the thickness of the brick units, r is the number of courses within the failing portion (assuming courses in the rocking portion), K_r is the overburden load (Equation 8), in which Q_r is the load per unit length on the top of the front wall, and γ_m is the volumetric weight of the masonry. The friction coefficient for adobe blocks varies from $\tan 30^\circ \approx 0.6$ (Corazao and Blondet 1973) to 1.09 (Tejada 2001).

$$\Omega_{pef} = 1.0 - 0.185 \frac{L}{h_s} \geq 0 \quad (7)$$

$$K_r = \frac{Q_r}{\gamma_m h_s} \quad (8)$$

IN-PLANE RESPONSE

When adobe walls are well connected, or have some buttresses, in-plane failure can be expected. That means that the walls can resist forces in their plane until diagonal cracks start to appear. Figure 8 shows a typical cracking pattern (X shape) due to the exceedance of the shear capacity in adobe walls.

In a similar manner to the out-of-plane behavior, the in-plane seismic capacity of the walls can be represented by a limit state displacement capacity; as mentioned before, this displacement is compared with the displacement demand from a response spectrum at the limit state period of vibration to ascertain whether the limit state is exceeded or not.

Limit States and Displacement Capacity

From the cyclic tests performed by Blondet et al. (2005), four limit states have been considered with different levels of drift (Figure 9). Observed structural damage is adopted as the main parameter to be considered for the limit state definition (Figure 10). Until 0.052% drift the structure can be considered elastic (LS1), which means fully operational. After that the structure may have some cracking but is still functional until 0.1% of drift (LS2). Then the life-safety performance (LS3) is reached at 0.26% of drift, and finally the structure is considered near collapse or collapsed at 0.52% of drift. These limit states are close to the

values proposed for unreinforced masonry buildings by Calvi (1999) and Javed (2008); however, it is recognized that additional laboratory tests on adobe walls are necessary to achieve more reliable values and associated uncertainty.

Five damage states can result from the limit state capacities discussed above (see Table 2).

Table 2. Description of damage for each limit state (adapted from Calvi 1999)

Description	Range
Nearly undamaged building, cracks up to 0.3 mm thick	Demand < LS1
Initiation diagonal cracks, usable building, cracks up to 0.6 mm thick	LS1 < Demand < LS2
Building extensively damaged but still repairable, horizontal cracks beginning, new cracks up to 1.6 mm thick	LS2 < Demand < LS3
Building not collapsed but with severe damage, continuation of horizontal cracks, cutting of adobe blocks, new cracks up to 5 mm thick	LS3 < Demand < LS4
Walls with crack larger than 5 mm thick, building collapse is expected	Demand > LS4

Displacement Capacity

The maximum displacement for a given limit state (Δ_{LS}) can be represented as the summation of the yield displacement Δ_y and the plastic displacement Δ_p (Equations 9, 10, and 11), which are obtained from knowing the interstory drift capacity of the walls at the yield and ultimate limit states (δ_y and δ_{LS} , respectively).

$$\Delta_y = k_1 \cdot \delta_y \cdot h_T \quad (9)$$

$$\Delta_p = k_2 \cdot (\delta_{LS} - \delta_y) \cdot h_{sp} \quad (10)$$

$$\Delta_{LS} = \Delta_y + \Delta_p \quad (11)$$

where h_T is the height of the story and h_{sp} is the height of the pier.

The coefficients k_1 (≈ 0.80) and k_2 (≈ 0.95) take into account the conversion from a multi-degree-of-freedom (MDOF) system to a SDOF system and they depend on the mass distribution and the effective height of the piers going into the inelastic range, h_{sp} (Restrepo-Velez and Magenes 2004). The general procedure is based on the SDOF substitute structure model proposed by Shibata and Sozen (1976).

Period of Vibration

Estimates of the elastic period of vibration of adobe buildings were obtained from two experimental tests carried out at the Catholic University of Peru (PUCP). The first test was a displacement controlled cyclic test carried out on an adobe wall by Blondet et al. (2005). The wall had an I-shape configuration (see Figure 11a) and it was built over a reinforced concrete foundation beam. At the top, a reinforced concrete crown beam was built to provide the gravity loading corresponding to a roof composed of wooden beams, cane, straw, mud, and corrugated zinc sheet. The period of vibration in this case was estimated to be around 0.14 s. The second test was a dynamic one performed over the unidirectional shake table of the PUCP on a full-scale adobe module (Blondet et al. 2006, Figure 11b), as with the previous test, the module was built over a reinforced concrete foundation beam. Here, a period of vibration of around 0.15 s was obtained directly from a free vibration test.

The periods of vibration obtained from the experimental test results were compared with the results of numerical analyses performed with the structural program SAP2000 (CSI 2005), for different configurations of adobe buildings (Figure 12). A reduced Young's modulus, $0.6E$, was used for the computation of elastic vibration periods, considering that at the first limit state the adobe walls were already cracked due to shrinkage, changes in environmental conditions, lack of maintenance, etc. As can be observed from the results of Figure 13, a good correlation between the period of vibration and the building height was observed (Tarque 2008).

A best-fit regression analysis was applied to the data shown in Figure 13 to obtain a vibration period versus building height, H , formula of the form $T = \alpha H^\beta$ (Goel and Chopra 1997), which led to the following expression: $T_y = 0.09H^{3/4}$.

The limit state period (T_{LSi}) can be obtained from the secant stiffness to the point of maximum deflection on an idealized bilinear force-displacement curve (Figure 14) as reported in Equation (12) (and described further in Crowley et al. 2004).

$$T_{LSi} = T_y \sqrt{\mu_{LSi}} \quad (12)$$

Evaluation of Equivalent Viscous Damping in Adobe Walls

In contrast to the out-of-plane behavior, the damping values for the in-plane mechanism will change for each limit state due to the process of damage. The equivalent viscous damping ratio for adobe walls has been calculated considering the energy absorbed in a

hysteretic loop (steady-state cyclic response) due to a given displacement level (limit state). In this case, the equivalent viscous damping will be evaluated for each limit state with Equation (13):

$$\xi_{hyst} = \frac{A_h}{4 \cdot \pi \cdot A_e} \quad (13)$$

where A_h is the dissipated energy within a complete cycle of stabilized force-displacement response, and A_e is the elastic energy related to the maximum force and displacement achieved in the stabilized loops (see Priestley et al. 2007). Typically, the dissipated energy in each cycle evolves with the increase of damage and the increase of displacement demand (Magenes and Calvi 1997). By evaluating the adobe wall tested by Blondet et al. (2005), two values of equivalent damping were computed for each limit state using the first and second cycle of each hysteretic curve. More details concerning the computation of damping ratios can be found in Tarque (2008). The resulting values related to each of the drift limits are summarized in Table 3. The assumed standard deviation values are given in Table 4 (see Borzi et al. 2008, Restrepo-Velez 2004).

Table 3. Limit states for adobe buildings

Limit state	Description	Drift (δ_{LS})	ζ (%)	Ductility
LS1	Operational	0.052%	10	1
LS2	Functional	0.10%	10	2
LS3	Life-safety	0.26%	12	5
LS4	Near or collapsed	0.52%	16	10

Reduction of the Demand

As the displacement-based method applied herein for in-plane response is based on an equivalent linear SDOF system, the demand spectrum needs to be represented at higher levels of damping to account for the nonlinear behavior of the system. In order to modify the 5% DRS for these higher levels of damping, the modification factor proposed by Priestley et al. (2007) has been used:

$$\eta = \sqrt{\frac{7}{2 + \xi}} \quad (14)$$

where the equivalent viscous damping, ξ , is given in %.

CHARACTERISTICS OF ADOBE DWELLINGS IN CUSCO

The typology of adobe dwellings in Cusco has been established according to a survey undertaken by Blondet et al. (2004) and by the 2007 Peruvian Census (INEI 2007). The location of Cusco in Peru is shown in Figure 15. It can be seen that around 76% of the houses are made of adobe, and at least 54% of them have just one story.

In Peru, the total number of earthen dwellings (adobe and *tapial*) forms an important percentage of the total number of Peruvian houses (INEI 2007). According to the last census (INEI 2007), the number of earthen buildings in Peru decreased from 43% to 35% of the total housing stock (Figure 16a) from 1993 to 2007.

However, adobe houses still comprise 76% of the total housing stock in the region of Cusco (which has more than 1,171,500 inhabitants) (Figure 16b), though the percentage in the province of Cusco (which has more than 348,500 inhabitants) has decreased slightly, from just over 80% in 1993 to around 68% in 2007 (Figure 16c). Despite this slight reduction, it is clear that people in Cusco build with adobe as a principal material and with clay bricks as a second material of choice.

According to Carazas (2001), construction in the rural area of Cusco (corresponding to the periphery of the city) has a strong pre-Hispanic influence, namely, most dwellings are single-story adobe dwellings with two rooms; one room is used for social activities, such as cooking or eating, and the other is generally used as a bedroom. Considering this statement and the information in Figure 17a, it may thus be concluded that in the region of Cusco more than 54% of adobe dwellings have one story.

GEOMETRIC PROPERTIES

Blondet et al. (2004) carried out a building survey in Cusco collecting information from a sample size of 30 adobe buildings (Figure 18, see Tarque 2008 for photos of these buildings). The data collected included dimensions of the walls and bricks, height of the gable, number of rooms, number of openings, etc. With that data it was possible to define the mean values and standard deviations of these geometric properties. For example, it was found that the mean wall thickness of adobe buildings in Cusco is 0.44 m, and the mean wall height is 2.45 m for single-story buildings and 4.88 m for two-story buildings. These mean heights have been calculated without considering the height of the gables. The thickness of the walls is fairly uniform among the buildings analyzed, which is confirmed by the low standard

deviation (0.04 m, see Table 4). It is important to remark that in other Peruvian cities, especially those located on the Peruvian coast, the wall thickness of adobe dwellings is around 0.25 m, which results in slenderness values (height/thickness ratio) greater than 9 and increases the probability of collapse through out-of-plane mechanisms. Adobe houses in Cusco have slenderness ratio values of around 6 and thus should be less susceptible to out-of-plane collapse.

The variability of each of the parameters in this study (i.e., wall lengths, adobe brick dimensions, etc.) can be represented by histogram plots which can then be fit to a probability density function (PDF). Figure 19 shows the histograms and the best-fit PDF for some of the geometric parameters.

It seems that continuous probability distributions such as the normal or lognormal distribution can represent fairly well some of the geometric properties (e.g., Figure 19a and 19b); on the other hand, some properties require discrete distributions (e.g., Figure 19c and 19d).

GENERATION OF RANDOM DATA

Using an adaptation of the software developed for the DBELA methodology (Crowley et al. 2006) it was possible to generate an artificial stock of 1,000 buildings with Monte Carlo simulation. The input data (based on the statistics of the 30 adobe dwellings; Blondet et al. 2004) was represented by the mean and standard deviation values of the principal geometric properties (Table 4) and by the best-fit for the probability density functions (e.g., lognormal, normal, uniform, and discrete distributions). The overburden load for typical adobe dwellings is computed in Tejada (2001). The standard deviation values for the limit states has been taken as 30% of the mean values (Borzi et al. 2008). Some parameters were available as integer values, thus a discrete distribution was used (Table 5).

The capacity equations for the in-plane and the out-of-plane behavior that have been described previously are used to calculate the displacement capacity and the respective period of vibration for different limit states for each of the 1,000 randomly generated buildings.

Table 4. Random variables used in DBELA for the definition of structural capacity of adobe dwellings

Description	Variable	Mean (μ)	Standard deviation (σ)	Distribution
In-plane failure mechanism				

Inter-story height (m)	h_p	2.45	0.21	Lognormal
Pier height (m)	h_{sp}	2.45	0.21	Lognormal
Period coefficient	C_I	0.088	0.004	Normal
Drift limit state 1	LS1	0.00052	0.000156	Lognormal
Drift limit state 2	LS2	0.001	0.0003	Lognormal
Drift limit state 3	LS3	0.0026	0.000578	Lognormal
Drift limit state 4	LS4	0.0052	0.00156	Lognormal
Out-of-plane failure mechanism				
Wall width (m)	t	0.44	0.04	Lognormal
Wall length (m)	L	4.53	0.59	Lognormal
Staggering length (m)	s	0.103	0.008	Lognormal
Thickness of brick units (m)	b	0.44	0.04	Lognormal
Height of brick units (m)	h	0.152	0.01	Lognormal

Table 4. Random variables used in DBELA for the definition of structural capacity of adobe dwellings (continuation)

Description	Variable	Mean (μ)	Standard deviation (σ)	Distribution
Out-of-plane failure mechanism				
Overburden load (kN/m)	Q_r	6.7	---	---
Specific weight (kN/m ³)	γ_m	18	---	---
Reduction factor for Δ_u	ϕ	0.85	0.05	Normal
Friction coefficient	μ_s	0.80	---	---
Δ_1/Δ_u	ρ_1	0.12	0.01	Normal
Δ_2/Δ_u	ρ_2	0.4	---	---
# of edge and internal orthogonal walls	β	See Table 5a		Discrete
# of courses within the story height	r	See Table 5b		Discrete

Table 5. (a) Number of edge and internal orthogonal walls, (b) number of courses within the story height

a)

Number	Total	Cumulative
2	24	0.40
3	22	0.77
4	2	0.97
5	2	1.00

b)

Number	Total	Cumulative
12	1	0.04
13	1	0.08
14	7	0.35
15	22	0.77
16	2	0.85
17	4	1.00

SEISMIC DEMAND FOR FRAGILITY ASSESSMENT

DRS have been employed herein in order to calculate the displacement demand from the seismic action, which is compared with the displacement capacity at a given period of vibration in order to derive fragility curves. To study the influence of using different displacement spectral shapes on the analysis of fragility curves, six different displacement spectral shapes were studied herein: three uniform hazard spectra (UHS) obtained from a probabilistic seismic hazard assessment for the city of Cusco, a scenario spectrum based on the disaggregation results from the probabilistic seismic hazard assessment (PSHA) and calculated from the Atkinson and Boore (2003) ground-motion prediction equation (GMPE), and the code spectral shapes from Eurocode 8 and the Peruvian Seismic Code. In each of the six aforementioned cases, a number of DRS have been generated for increasing levels of intensity. A soil type with $180 < V_{S30} < 360 \text{ m/s}^2$ was used in all cases.

UNIFORM HAZARD SPECTRA - PROBABILISTIC SEISMIC HAZARD ASSESSMENT

Castillo and Alva (1993) have identified 20 seismic sources for Peru due to both subduction processes and crustal events. The subduction events are due to the interaction of the Nazca and South American plates where the former passes beneath the latter. The crustal events are related to the shallow earthquakes due to the compression stresses from the Peruvian highlands that result in the orogenic process of the Andes Cordillera (mountain).

The shallow subduction zone (Benioff zone, 0–70 km) is represented by the sources F1 to F5 located along the Peruvian coast (see Figure 20). The intermediate seismicity (71–300 km) is represented by sources F13 to F19, and the deep seismicity (500–700 km) is represented by source F20. The crustal events are represented by sources F6 to F12.

Three PSHAs for Cusco have been carried out herein taking into account different combinations of GMPEs. For each PSHA, around 50 uniform hazard acceleration response spectra (ARS) were calculated for different return periods, each of which can be associated with a unique PGA value.

The first PSHA (Y+S) considered the Youngs et al. (1997) attenuation for subduction seismic sources and the Sadigh et al. (1997) for crustal events. The second run (Y+BA) considered Youngs et al. (1997) for subduction seismic sources and Boore and Atkinson (2007) for crustal events. The last (AB+BA) considered the most recent GMPEs for both

subduction and crustal events, which are Atkinson and Boore (2003) and Boore and Atkinson (2007).

As discussed by Atkinson and Boore (2003), the ground motions predicted with their equation tend to be lower than those predicted with the equations by Youngs et al. (1997). For this reason it was expected that lower levels of hazard would be obtained for the AB+BA run (Figure 21a). Seismic hazard curves for Y+S and for Y+BA have more or less the same PGA value for each annual frequency of exceedance, which shows that the subduction sources are dominating the seismic hazard, as the change in GMPE for the areal sources has almost no influence. Figure 21b shows ARS for the three PSHA, which have all been normalized to the same PGA; it can be seen that the spectral shape depends on the GMPE used. The required DRS have been obtained by multiplying the acceleration spectra by $(T/2\pi)^2$.

SCENARIO SPECTRUM

Disaggregation of each of the three PSHAs has been carried for the PGA at a return period of 475 years and the results show that the controlling scenario was located around 120 km from Cusco (closest distance to rupture, R_{rup}) and with an M_w of 6.8, which corresponds to the intermediate subduction seismic source F16. A single scenario spectrum considering the Atkinson and Boore (2003) GMPE has thus been calculated. Many ARS were computed considering an M_w of 6.8 and varying the R_{rup} to produce spectra of different intensities.

EUROCODE 8

The acceleration spectral shape specified by Eurocode 8, henceforth referred to as EC8, (CEN 2005) has been anchored to increasing levels of PGA to generate a set of ARS that have then been multiplied by $(T/2\pi)^2$ to obtain the DRS. As was mentioned before, the reduction factor, η , due to damping values different than 5%, is computed by Equation 14. Following the recommendations of EC8, the displacement spectra have been taken as constant after 2 s.

$$0 \leq T < T_B : \quad S_e(T) = a_g \cdot S \left(1 + \frac{T}{T_B} \cdot (\eta \cdot 2.5 - 1) \right) \quad (15)$$

$$T_B \leq T < T_C : \quad S_e(T) = a_g \cdot S \cdot \eta \cdot 2.5 \quad (16)$$

$$T_C \leq T < T_D : \quad S_e(T) = a_g \cdot S \cdot \eta \cdot 2.5 \cdot \frac{T_C}{T} \quad (17)$$

$$T_D \leq T \leq 4s : \quad S_e(T) = a_g \cdot S \cdot \eta \cdot 2.5 \cdot \frac{T_C \cdot T_D}{T^2} \quad (18)$$

where S_e are the values of the spectral accelerations; a_g is the PGA value; S is the soil factor; T_B , T_C , and T_D are the characteristic periods of the spectral shape and depends on the ground type; and η is the damping correction factor, which should be 1 for the elastic response spectra.

In order to select the characteristic period values from EC8, it was necessary to know whether earthquakes occurring at the study zone have a magnitude that is higher or lower than M_w 5.5, because EC8 gives two different acceleration spectral shapes for magnitudes on either side of this value. Based on the disaggregation of the PSHA, it was decided to work with values of characteristic periods given by earthquakes greater than M_w 5.5 and for a C soil type ($180 < V_{S30} < 360$ m/s²), which means a soil factor of $S = 1.15$. The resulting values for T_B , T_C , and T_D were 0.2, 0.6, and 2 s, respectively. The damping correction factor was defined as a function of the equivalent viscous damping obtained from Equation 14.

PERUVIAN SEISMIC CODE

The equations to evaluate the acceleration response spectrum in the Peruvian seismic code (SENCICO 2003) are as follows:

$$Sa = \frac{Z \cdot U \cdot S \cdot C}{R} g \quad (19)$$

$$C = 2.5 \cdot \frac{T_P}{T} \leq 2.5 \quad (20)$$

where Sa are the values of the spectral accelerations, Z is the expected PGA, U is a factor that depends on the importance of the building, S is the soil factor, C is the seismic amplification factor and should be less than 2.5, R is a reduction factor, and T_P is the period corresponding to the end of the plateau zone.

For houses, U is equal to 1 and the soil type in Cusco has been classified as intermediate soil regarding the Peruvian Seismic Code, which is close to the soil type C given by EC8, and thus the soil factor is equal to 1.2 and T_P is 0.6 s for intermediate soils. The acceleration

spectral ordinate for $T = 0$ s does not give the PGA value (as is the case in the EC8 spectrum). For this reason the ARS shape starts directly from a plateau zone up to T_p .

As the Peruvian code does not specify the corner period for DRS, from where the displacement is constant, the acceleration spectra have been directly transformed to displacement spectra even past 2 s.

COMPARISON OF RESPONSE SPECTRAL SHAPES

Figure 22 shows six acceleration spectral shapes and the related displacement spectral shapes evaluated from the two seismic design codes, the three UHS (from PSHA, where Y+S and Y+BA are superimposed on top of each other), and the scenario spectrum. For graphical reasons all spectra have been anchored to a common PGA value of 0.17 g, which has been evaluated for $M_w = 6.8$ and $R_{rup} = 120$ km with the Atkinson and Boore (2003) GMPE. It can be seen in Figure 22b that for the range of periods of vibration corresponding to the out-of-plane response of walls (close to 2 s), the highest displacement demand is due to the two seismic codes, while the lowest is given by the scenario spectrum. The same trend is also seen in Figure 22c over the range of periods of vibration for the in-plane behavior of walls (from 0.15 to 0.6 s).

FRAGILITY CURVES FOR ADOBE DWELLINGS IN CUSCO

Fragility curves, in terms of PGA, calculated for each limit state with the six different displacement spectral shapes, considering both in-plane and out-of-plane failure mechanisms, have been calculated using the procedure described earlier and are shown in Figures 23 and 24, respectively. The adobe buildings generated herein have in-plane limit state periods of vibration between 0.15 and 0.6 s and an out-of-plane limit state period of vibration close to 2 s; the difference in the DRS in these regions should be reflected in the fragility curves.

For the in-plane response, for all levels of intensity, the highest vulnerability is given by the two spectra from the design codes, followed by the UHS Y+S and Y+BA, then AB+BA and, finally, the scenario spectrum which gives the lowest fragility, as seen in Figure 23. Out-of-plane fragility curves follow the same trend as the ones from the in-plane case, as can be seen in Figure 24; the only difference is that fragility curves evaluated with AB+BA give higher probabilities of failure than the ones computed with Y+S and Y+BA.

Fragility curves have also been calculated in terms of spectral displacement. In this case the probability of exceedance, which is calculated by comparing the displacement demand with the displacement capacity, is plotted against the mean spectral displacement demand to the randomly generated set of buildings. The mean spectral displacement demand is obtained from the displacement spectrum at the mean limit state period of vibration. The mean limit state periods of vibration for the in-plane response were 0.17 s, 0.25 s, 0.41 s, and 0.59 s for limit states 1, 2, 3, and 4, respectively. For the out-of-plane mechanism, the mean period of vibration for the ultimate limit state was 1.95 s. Figure 25 shows the fragility curves obtained for the various spectra considered herein when the probability of exceedance is plotted against the mean limit state displacement demand, for LS4. It is evident that the spectral shape has a negligible influence on the results in this case. The reason is that for a given mean displacement demand, the variation of the spectral shape over the range of periods of the random population of buildings is minimal, as illustrated in Figure 26, consequently, very close probabilities of failure are computed regardless of the spectral shape.

Figure 27 presents the fragility curves obtained in the manner described above for both in-plane and out-of-plane responses. It is noted that should one want to use these fragility curves within a risk assessment, it would be necessary to obtain the seismic hazard in terms of the mean limit state periods of vibration for the two mechanisms (in-plane and out-of-plane) which were reported above. Hence, for example, in order to assess the probability of in-plane collapse (LS4) based on a given displacement response spectrum, the user should calculate the displacement demand at a period of vibration of 0.59 s, which is the mean limit state period for LS4, and then enter Figure 27a at this displacement demand to calculate the probability of exceedance of LS4.

Figure 28 shows the procedure described before. In this case, the EC8 displacement response spectrum has $PGA = 0.1$ g. The resulting spectral displacement for the mean period of vibration LS3 is 0.0085 m (Figure 28a). The probability of exceedance obtained from Figure 28b is around 92% for LS3. It is important to note that the displacement response spectrum should be affected by the modification factor η (Equation 14) if the damping ratio is different from 5% (CEN 2005).

In 1950 a big earthquake shook Cusco city. At that time no acceleration data was recorded; however, a PGA of 0.3 g was estimated by Ericksen et al. (1954) and it was reported that more than 63% of dwellings (not necessarily earthen dwellings) had to be

reconstructed. Since it was not possible to obtain the displacement response spectrum associated to the earthquake, Figure 23d was used to estimate the probability of exceedance of LS4. The curves obtained (except the one computed from the Atkinson and Boore GMPE) show that for a 0.3 g earthquake, 100% of the earthen buildings could exceed the in-plane LS4. For the out-of-plane mechanism (Figure 24) and considering the Peruvian spectral shape, it is observed that almost 100% of the buildings have exceeded the LS_u .

APPLICATION OF FRAGILITY CURVES FOR ADOBE DWELLINGS IN PISCO

On 15 August 2007, an earthquake of M_w 8.0 occurred on the central coast of Peru, with an epicenter near to Pisco city. According to the National Institute of Civil Defense (INDECI, a Peruvian governmental institute) there were 593 casualties, 48,208 dwellings completely collapsed, and 45,500 were left uninhabitable. In Pisco alone there were 31,011 affected dwellings out of a total of 36,232. The adobe dwellings were the most affected structures and it is estimated that all of these structures suffered damage (Blondet et al. 2008). Pisco is a city located on the coast, with sand as a predominant soil type. According to the 2007 Census (INEI 2007), the earthen dwellings built with adobe or *tapial* form 19.81% of the total dwellings in Pisco, small buildings constructed using mats form 23.27%, and masonry dwellings comprise 43.60%.

In order to attempt to verify the methodology proposed here, fragility curves for Pisco city have been computed. It is important to remark that there is no precise information on the geometric properties for adobe dwellings in Pisco; however, some of them were taken from the adobe modules tested at the PUCP, which aim to represent typical dwellings located on the Peruvian coast. Table 6 shows just the input values that have been modified from Tables 4 and 5 in order to generate an artificial building stock for Pisco.

Table 6. Updated random variables used in DBELA for the definition of structural capacity of adobe dwellings from Pisco

Description	Variable	Mean (μ)	Standard deviation (σ)	Distribution
In-plane failure mechanism				
Inter-story height (m)	h_p	2.10	0.20	Lognormal
Pier height (m)	h_{sp}	2.10	0.20	Lognormal
Out-of-plane failure mechanism				
Wall width (m)	t	0.30	0.05	Lognormal
Wall length (m)	L	3.75	0.25	Lognormal

Thickness of brick units (m)	b	0.30	0.05	Lognormal
Height of brick units (m)	h	0.11	0.01	Lognormal

Number of edge and internal orthogonal walls

Number	Cumulative
2	0.80
3	1.00

Number of courses within the story height

Number	Cumulative
14	0.08
15	0.35
16	0.77
17	0.85
18	1.00

The fragility curves shown in Figure 29 are expressed in terms of spectral displacement and have been computed taking into account the Peruvian code, the EC8 code, and a UHS based on Y+BA GMPEs, in all cases considering the soil characteristics of Pisco. The closest station to Pisco city, called ICA2, is located around 40 km away from Pisco, where the soil type is silty sand with a shear wave velocity of around 100 km/s (Bernal and Tavera 2007). For the purpose of this study, the record from Station ICA2 will be taken as representative for Pisco city. Figure 30 shows the elastic acceleration and DRS computed from the record. It seems that the N–S component, which is parallel to the fault, has more amplification than the E–W component. The mean value of these two components will be used for analyzing the spectral displacement values related to the mean period of vibration of the adobe dwellings.

From the building stock, the mean periods of vibration for the in-plane capacity were found to be 0.15, 0.22, 0.37, and 0.52 s, for LS1, LS2, LS3, and LS4, respectively. For the out-of-plane capacity, the mean period of vibration for LS_u was 1.75 s. The elastic DRS shown in Figure 30b should be multiplied by the modification factor η (Equation 13) in order to represent the higher levels of damping for the in-plane analysis. For the out-of-plane, the elastic DRS should be scaled by 1.5 for comparison with the displacement capacity (Griffith et al. 2005). These scaled DRS are showed in Figure 31 and should be used to obtain the spectral displacements (S_d) representative of the Pisco earthquake. The values for S_d were 0.0026, 0.0062, 0.020, and 0.038 m for LS1, LS2, LS3, and LS4, respectively, considering the in-plane analysis, and 0.33 m for LS_u considering the out-of-plane analysis.

The probabilities of exceedance for each limit state have been obtained from Figure 29, having as an input data the S_d computed from the Pisco earthquake. In all cases the fragility curves indicate that all (i.e., 100%) of the adobe dwellings in Pisco would have exceeded LS4

and LS_u for in-plane and out-of-plane capacity, respectively. The results are conservative, but it is highlighted that in order to derive stable conclusions on the validity of the proposed method for adobe structures it would be necessary to have more recordings from the Pisco earthquake in the regions where damage was experienced.

CONCLUSIONS

This paper has focused on the analysis of the seismic capacity of adobe dwellings (single-story) in order to evaluate fragility functions. Displacement capacity formulae, limit states, and period-height relationships have been derived.

The in-plane and out-of-plane capacity of adobe walls is expressed in terms of limit state displacement and the related period of vibration. Four limit states (LS) have been given for the in-plane behavior (based on a cyclic test carried out at the PUCP) and one LS for the out-of-plane response. The LSs for the former are given in terms of drifts: 0.052%, 0.1%, 0.26%, and 0.52% used in the analysis with a coefficient of variation (COV) of 30%. The LS for the out-of-plane response is related to wall thickness and defines the complete overturning of a parapet wall. Experimental results of adobe building specimens constructed and tested on a reaction floor/frame system and on a shake table at the PUCP, and from analytical models of adobe buildings have been used to study the period of vibration of typical Peruvian adobe buildings as a function of height, H , leading to the following relationship: $T_y = 0.09H^{3/4}$. The typical roof of an adobe dwelling is composed of wooden beams, cane, straw, mud, and roof tiles or corrugated zinc sheet. This relation gives elastic vibration periods of vibration of around 0.15 s for single-story adobe buildings, and around 0.25 s for two-story adobe buildings. Further developments could be extended to include the influence of other parameters such as wall thickness and number of openings on the period of vibration.

An application of the methodology to buildings located in Cusco, Peru, as well as the analysis of the seismic demand expected for that zone has been computed. Fragility curves have been produced by generating a random population of adobe buildings based on the structural characteristics of these buildings in Cusco; the probability of exceedance of a given limit (or damage) state has been calculated from the comparison of the seismic capacity and the seismic demand of each random building, and this has then initially been related to a value of PGA to produce fragility curves. The strong influence of the GMPE and the earthquake magnitude on the spectral shape have meant that very different estimates of

fragility have been obtained for a given value of PGA. Should an engineer wish to carry out a risk analysis where the hazard is given only in terms of PGA, they should use a different fragility curve depending on how the hazard has been computed; for example, in this paper eight ARS shapes have been used.

It is noted that UHS should not really be used for fragility assessment as the spectral ordinates at the higher periods of vibration are produced by higher magnitude earthquakes than the ordinates at lower periods of vibration, and thus they do not give realistic representations of the response of a SDOF system whose period of vibration would increase under seismic action. This issue is outside the scope of this paper, but vector-valued PSHA where the joint hazard of multiple spectral ordinates are considered (e.g., Bazzurro and Cornell 2002) would be recommended instead.

Alternative fragility curves are proposed herein in terms of spectral displacement at the mean limit state period of vibration; these fragility curves are not influenced by the spectral shape as they directly relate the parameter used to define the limit state exceedance probability and the intensity of the ground shaking.

Future developments will include a more detailed study on the definition of limit states to damage for the in-plane and out-of-plane behavior of adobe buildings as well as the period of vibration of these buildings. Additionally, fragility curves that combine both failure modes should be derived following further analysis using nonlinear numerical models. Furthermore, the procedure will be applied to adobe buildings with different geometric characteristics within Peru, and should also be adapted to other building typologies found in other parts of the world.

ACKNOWLEDGEMENTS

The authors thank Dr. Marcial Blondet, from PUCP, for his collaboration during the development of this work and for providing the data from experimental tests. Furthermore, the comments of the anonymous reviewers are greatly acknowledged as they have helped to significantly improve the manuscript.

REFERENCES

- Atkinson, G. M., and Boore, D. M., 2003. Empirical ground-motion relations for subduction zone earthquakes and their application to Cascadia and other regions, *Bulletin of the Seismological Society of America* **93**, 1703–1729.
- Bariola, J., and Sozen, M., 1990. Seismic tests of adobe walls, *Earthquake Spectra* **6**, 37–56.
- Bazzurro, P., and Cornell, C. A., 2002. Vector-valued probabilistic seismic hazard analysis (VPSHA), Paper No. 61, *7th U.S. National Conf. on Earthquake Engineering*, 21–25 July 2002, Boston, MA.
- Bernal, I., and Tavera, H., 2007. Maximum acceleration registered in Ica City: The August 15 Pisco earthquake (in Spanish), *Geologic Society Bulletin*, Peruvian Geophysics Institute, Lima, Peru.
- Blondet, M., Tarque, N., and Acero, J., 2004. *Study of the Seismic Vulnerability of Nonengineered Buildings Located in the Peruvian Highlands* (in Spanish), National Service for the Construction Industry Capacitation (SENCICO)-Catholic University of Peru (PUCP) joint project, Lima, Peru.
- Blondet, M., Madueño, I., Torrealva, D., Villa-García, G., and Ginocchio, F., 2005. Using industrial materials for the construction of safe adobe houses in seismic areas, *Earth Build 2005 Conference*, 19–21 January 2005, Sydney, Australia.
- Blondet, M., Vargas, J., Torrealva, D., Tarque, N., and Velázquez, J., 2006. Seismic reinforcement of adobe houses using external polymer mesh, *First European Conference on Earthquake Engineering and Seismology ECEES*, 3–8 September 2006, Geneva, Switzerland.
- Blondet, M., Tarque, N., and Vargas, J., 2008. Behaviour of earthen structures during the Pisco earthquake, *14th World Conference on Earthquake Engineering*, 12–19 October 2008, Beijing, China.
- Boore, D. M., and Atkinson, G. M., 2007. Ground-motion prediction equations for the average horizontal component of PGA, PGV, and 5%-damped PSA at spectral periods between 0.01 s and 10.0 s, *Earthquake Spectra* **24**, 99–138.
- Borzi, B., Crowley, H., and Pinho, R., 2008. Simplified pushover-based earthquake loss assessment (SPBELA) method for masonry buildings, *International Journal of Architectural Heritage* **2**, 353–376.
- Calvi, G. M., 1999. A displacement-based approach for vulnerability evaluation of classes of buildings, *Journal of Earthquake Engineering* **3**, 411–438.
- Carazas, W., 2001. *Vivienda Urbana Popular de adobe en el Cusco* (in Spanish), United Nations Educational, Scientific and Cultural Organization (UNESCO), Grenoble, France.
- Castillo J., and Alva J., 1993. Seismic hazard in peru (in Spanish), *VII National Congress of Soil Mechanism and Engineering of Foundations*, 6–10 December 1993, Lima, Peru.

- European Committee for Standardisation (CEN), 2005. *Design of Structures for Earthquake Resistance, Part 1: General rules, seismic action and rules for buildings, Eurocode 8, ENV-1998-1-1*, Brussels, Belgium.
- Corazao, M., and Blondet, M., 1973. *Experimental Study of the Structural Behaviour of Adobe Buildings Due to Seismic Solicitations*, Division of Civil Engineering, Catholic University of Peru, Lima, Peru.
- Crowley, H., Pinho, R., and Bommer, J., 2004. A probabilistic displacement-based vulnerability assessment procedure for earthquake loss estimation, *Bulletin of Earthquake Engineering* **2**, 173–219.
- Crowley, H., Pinho, R., Bommer, J., and Bird, J., 2006. *Development of a Displacement Based Method for Earthquake Loss Assessment*, European School for Advanced Studies in Reduction of Seismic Risk (ROSE School), Istituto Universitario di Studi Superiori di Pavia (IUSS) Press, Pavia, Italy.
- Computers and Structures Inc. (CSI), 2005. Structural Analysis Program: SAP v10.01, Berkeley, CA.
- D'Ayala, D., and Speranza, E., 2003. Definition of collapse mechanisms and seismic vulnerability of historic masonry buildings, *Earthquake Spectra* **19**, 479–509.
- Doherty, K., Griffith, M. C., Lam, N., and Wilson, J., 2002. Displacement-based seismic analysis for out-of-plane bending of unreinforced masonry wall, *Journal of Earthquake Engineering and Structural Dynamic* **31**, 833–850.
- Ericksen, G., Fernandez, J., and Silgado, E., 1954. The Cusco, Peru, earthquake of May 21, 1950, *Bulletin of the Seismological Society of America* **44**, 97–112.
- Goel, R., and Chopra, A., 1997. Period formulas for moment-resisting frame buildings, *Journal of Structural Engineering ASCE* **123**, 1454–1461.
- Griffith, M. C., Magenes, G. M., Melis, G., and Picchi, L., 2003. Evaluation of out-of-plane stability of unreinforced masonry walls subjected to seismic excitation, *Journal of Earthquake Engineering* **7**, Special Issue No. 1, 141–169.
- Griffith, M. C., Lam, M., and Wilson, J., 2005. Displacement-based assessment of the seismic capacity of Unreinforced Masonry walls in bending, *Australian Journal of Earthquake Engineering* **6**, 119-132.
- National Institute of Statistic and Informatics (INEI), 2007. Census 2007, www.inei.gob.pe.
- Javed, M., 2008. *Seismic Risk Assessment of Unreinforced Brick Masonry Building System of Northern Pakistan*, Ph.D. Thesis, Civil Engineering Dept. (NWFP University of Engineering and Technology Peshawar, Pakistan).

- Magenes, G., and Calvi, G. M., 1997. In-plane seismic response of brick masonry walls, *Journal of Earthquake Engineering and Structural Dynamics* **26**, 1091–1112.
- Melis, G., 2002. *Displacement-Based Seismic Analysis for Out-of-Plane Bending of Unreinforced Masonry Walls*, Master's Dissertation, European School for Advanced Studies in Reduction of Seismic Risk (ROSE School), University of Pavia, Italy.
- Priestley, M. J. N., Calvi, G. M., and Kowalsky, M. J., 2007. *Displacement-Based Seismic Design of Structures*, Istituto Universitario di Studi Superiori di Pavia (IUSS) Press, Pavia, Italy.
- Restrepo-Velez, L., 2004. *Seismic Risk of Unreinforced Masonry Buildings*, Doctoral Thesis, European School for Advanced Studies in Reduction of Seismic Risk (ROSE School), University of Pavia, Italy.
- Restrepo-Velez, L., and Magenes, G., 2004. Simplified procedure for the seismic risk assessment of unreinforced masonry buildings, Paper No. 2561, *13th World Conference on Earthquake Engineering*, 1–6 August, Vancouver, Canada.
- Tarque, N., 2008. *Seismic Risk Assessment of Adobe Dwellings*, European School for Advanced Studies in Reduction of Seismic Risk (ROSE School), University of Pavia, Italy, http://www.roseschool.it/index.php?option=com_docman&task=doc_download&gid=183&mode=view, accessed October 2009.
- Sadigh, K., Chang, C. Y., Egan, J., Makdisi, M., and Youngs, R. R., 1997. Attenuation relationships for shallow crustal earthquakes based on California strong motion data, *Seismological Research Letters* **68**, 180–189.
- National Service for the Construction Industry Capacitation (SENCICO) 2003. – *Technical Standard of Building NTE E030 - Earthquake Resistant Design* (in Spanish), Lima, Peru.
- Shibata, A., and Sozen, M. A. 1976. Substitute structure method for seismic design in R/C, *Journal of the Structural Division*, ASCE **102**, 1–18.
- Tejada, U., 2001. *Buena Tierra, apuntes para el diseño y construcción con adobe* (in Spanish), Centre of Researching, Documentation and Consultant Assistance (CIDAP), Lima, Peru.
- Youngs R. R., Chiou S., Silva W., and Humphrey J., 1997. Strong ground motions attenuation relationships for subduction zone earthquakes, *Seismological Research Letters* **68**, 58–73.

FIGURES

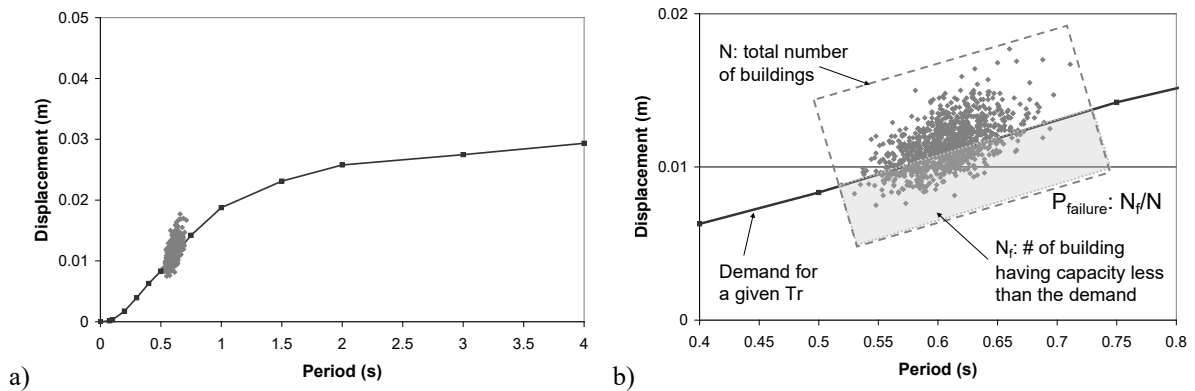


Figure 1. (a) Example of capacity versus demand comparison for a given response spectrum, (b) detail of Figure 1a.



Figure 2. Vertical cracks at the corners of connecting adobe walls.

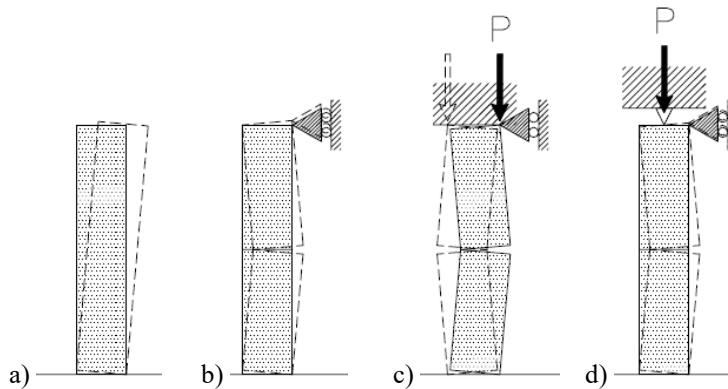


Figure 3. Unreinforced masonry wall support configurations (adapted from Griffith et al. 2003): (a) parapet wall, (b) simply-supported non-load-bearing wall, slip joint boundary condition, (c) simply-supported load-bearing wall, slab boundary condition, (d) simply-supported load-bearing wall, timber bearer boundary condition.

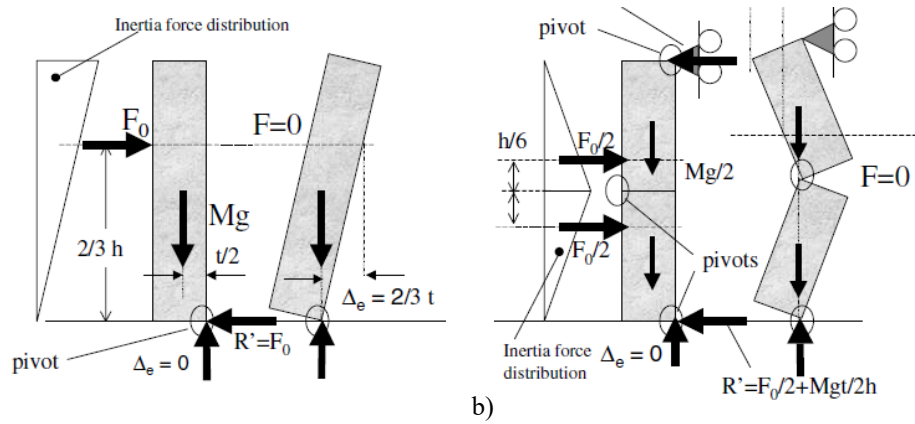


Figure 4. Inertia forces and reactions on rigid URM walls at incipient rocking and point of instability: (a) parapet wall, (b) simply-supported wall (Doherty et al. 2002).

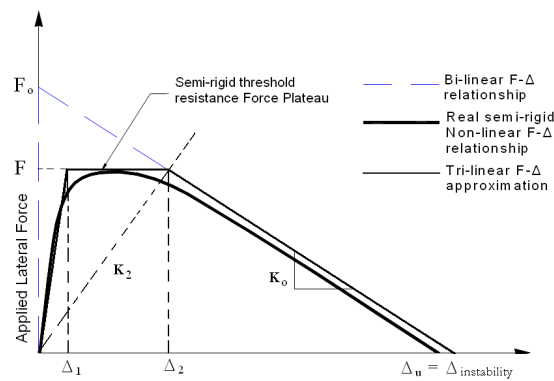


Figure 5. Trilinear idealization of the static force-displacement curve (adapted from Griffith et al. 2003).

A	B1	B2	C	D	E
VERTICAL OVERTURNING	OVERTURNING WITH 1 SIDE WING	OVERTURNING WITH 2 SIDE WINGS	CORNER FAILURE	PARTIAL OVERTURNING	VERTICAL STRIP OVERTURNING

Figure 6. Typical collapse mechanisms for URM buildings (D'Ayala and Speranza 2003).

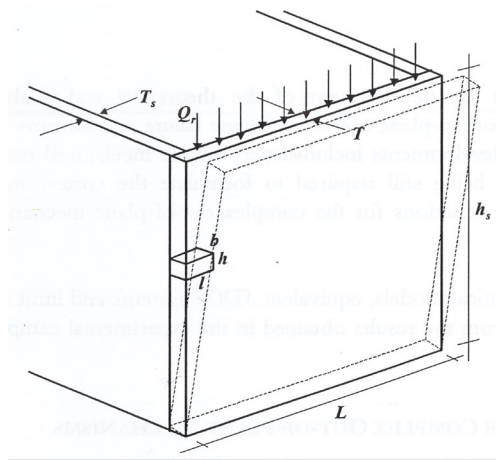


Figure 7. Failure Mechanism A, out-of-plane (Restrepo-Velez 2004).



Figure 8. Failure of walls due to in-plane forces (see Table 2): (a) demand < LS4, (b) demand > LS4.

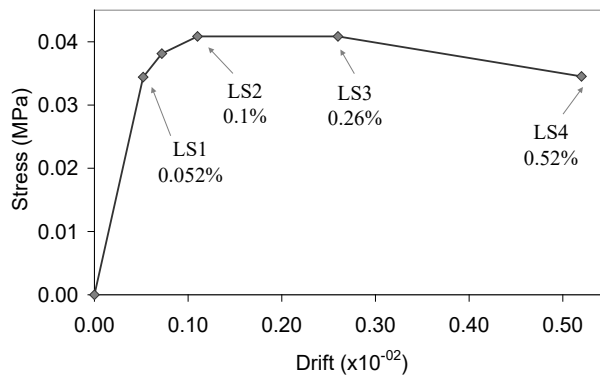


Figure 9. Capacity curve for an adobe wall subjected to in-plane loadings.

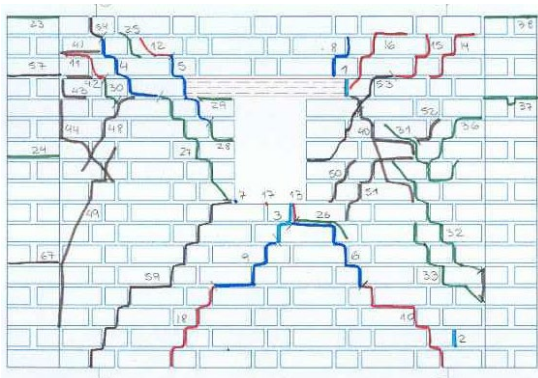


Figure 10. Cyclic test (Blondet et al. 2005), front view of the wall after testing.

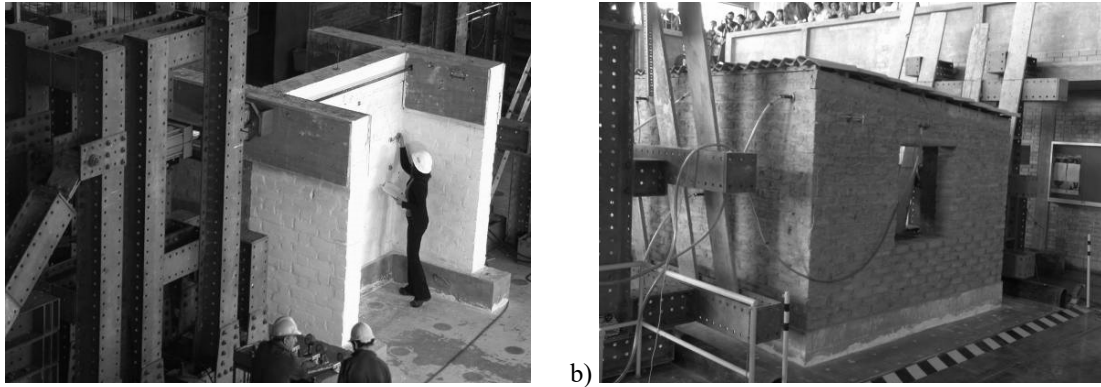


Figure 11. (a) Cyclic test (Blondet et al. 2005), (b) dynamic test (Blondet et al. 2006). Tests carried out at the Catholic University of Peru.

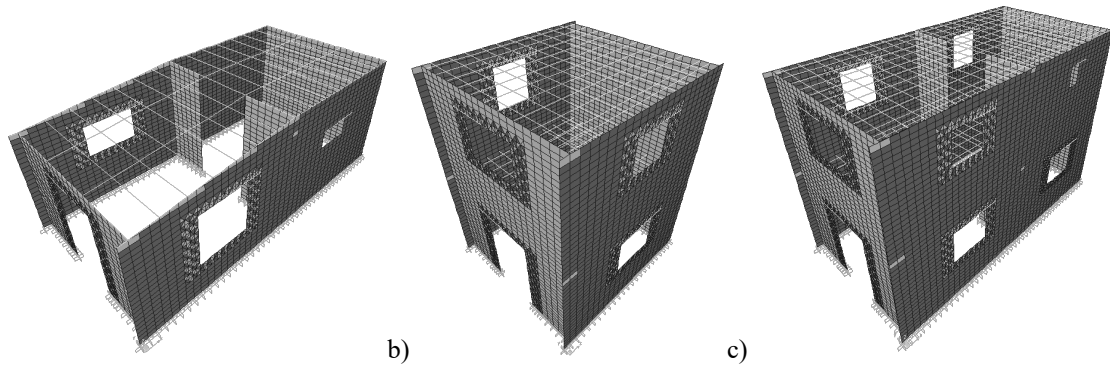


Figure 12. Analytical model for: (a) single-story building with two rooms, (b) two-story buildings with two rooms, (c) two-story buildings with four rooms.

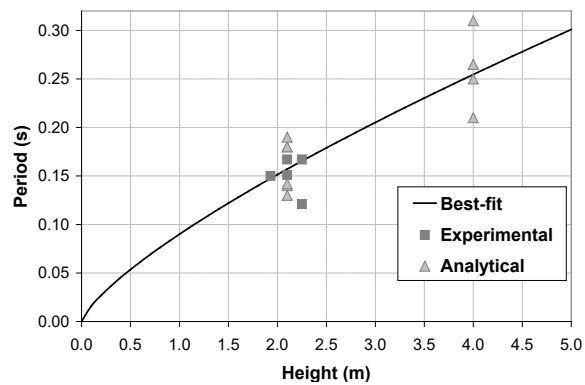


Figure 13. Vibration period versus building height (experimental and analytical data and best-fit regression curve).

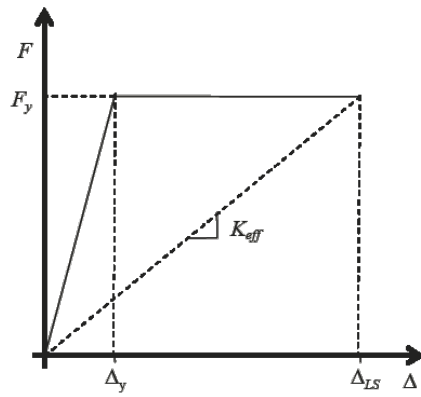


Figure 14. Elasto-plastic force displacement relationship.

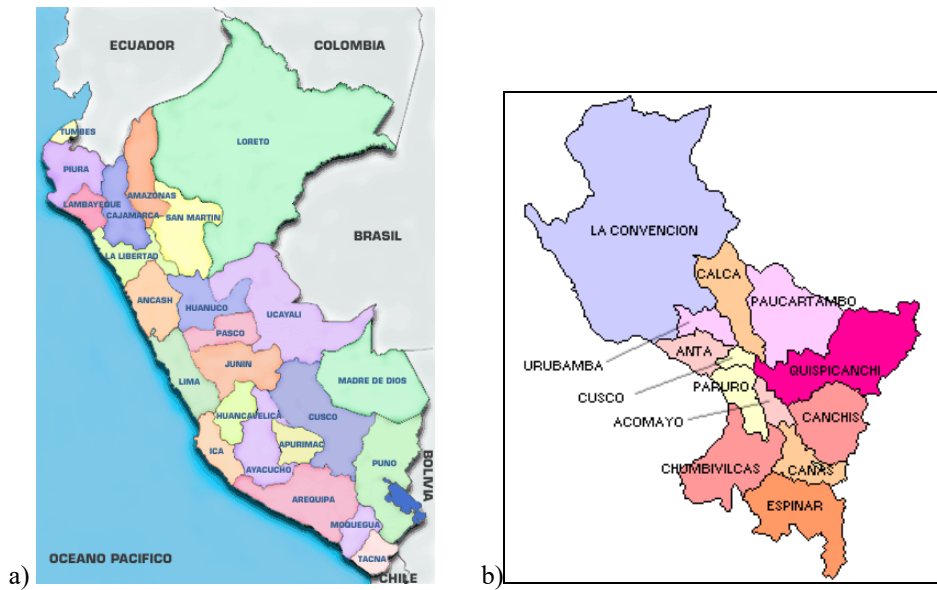


Figure 15. Political division of Peru and Cusco region: (a) regions of Peru (<http://www.go2peru.com>); (b) Cusco's regions and its provinces (<http://www.perucusco.com/080000.gif>).

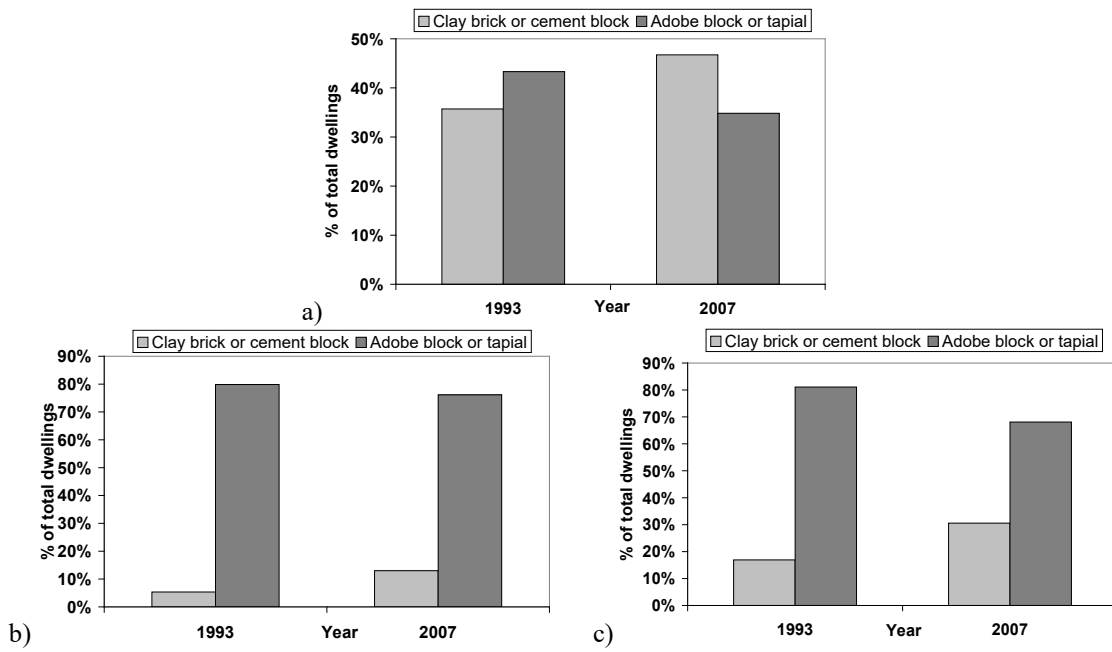


Figure 16. Percentage of adobe and clay brick masonry buildings in 1993 and 2007 (INEI 2007): (a) Peru, 6,400,131 dwellings; (b) region of Cusco, 293,584 dwellings; (c) province of Cusco, 88,337 dwellings.

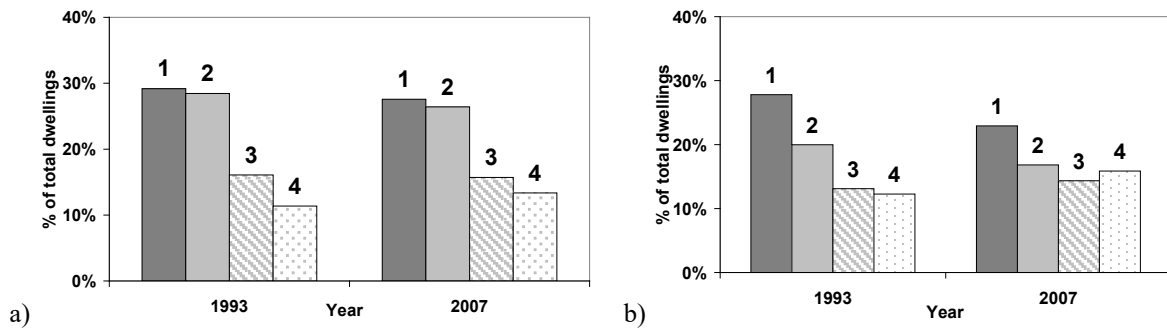


Figure 17. Number of rooms in adobe dwellings (INEI 2007): (a) Region of Cusco, (b) province of Cusco.



Figure 18. Adobe buildings in Cusco: (a) <http://www.downtheroad.org>, (b) Blondet et al. (2004).

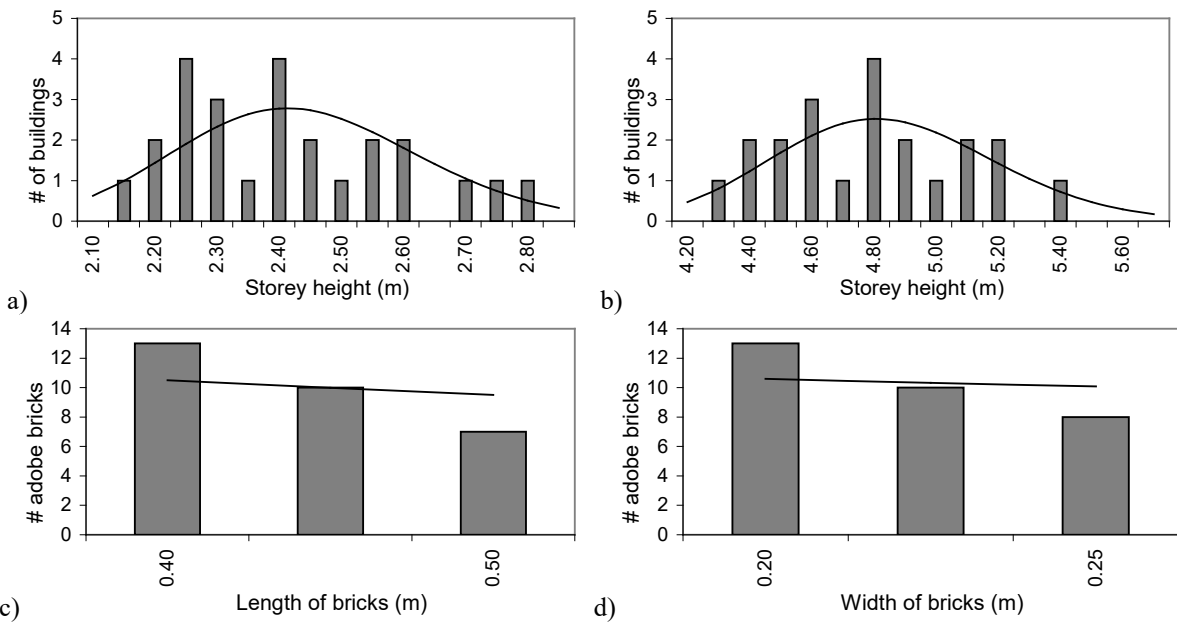


Figure 19. Histograms and PDFs for mean geometric properties: (a) Height of single-story buildings, (b) height of single-story buildings, (c) brick length, (d) brick width.

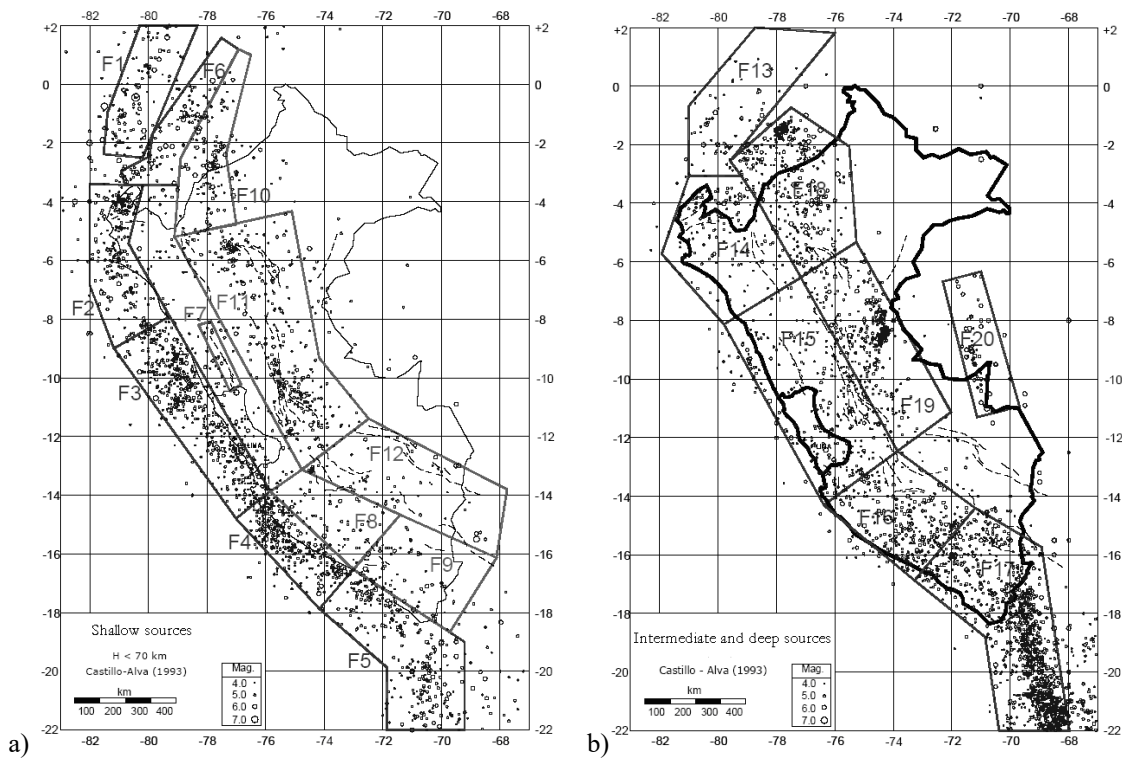


Figure 20. Peruvian seismic sources: (a) shallow subduction and crustal sources, (b) intermediate and deep subduction seismic sources (adapted from Castillo and Alva 1993).

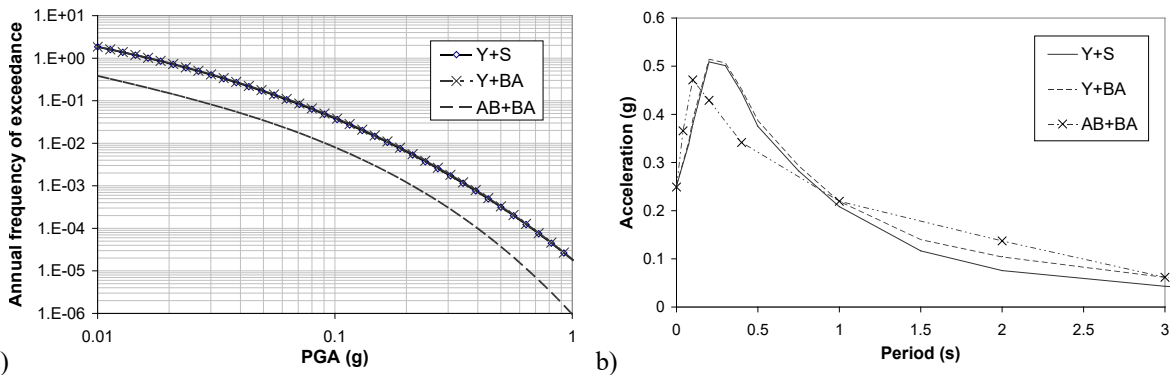


Figure 21. (a) Seismic hazard curves, (b) acceleration response spectra.

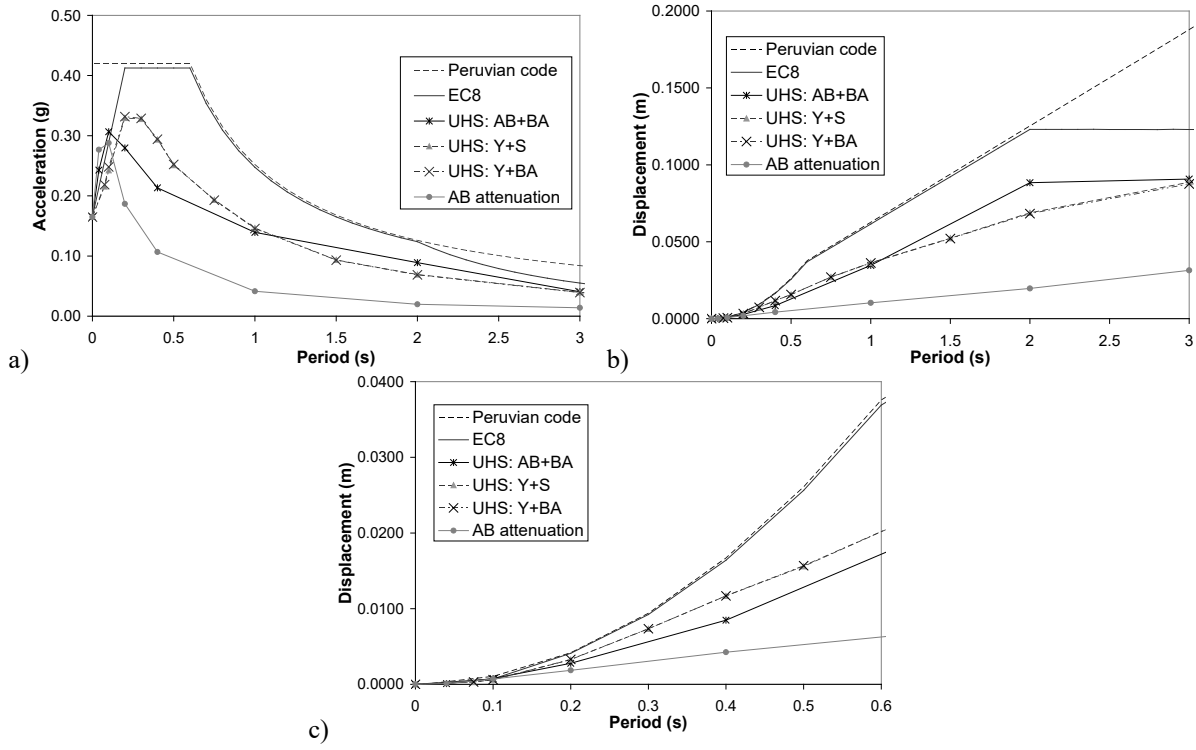


Figure 22. (a) ARS, (b) DRS, (c) detail of Figure 22b.

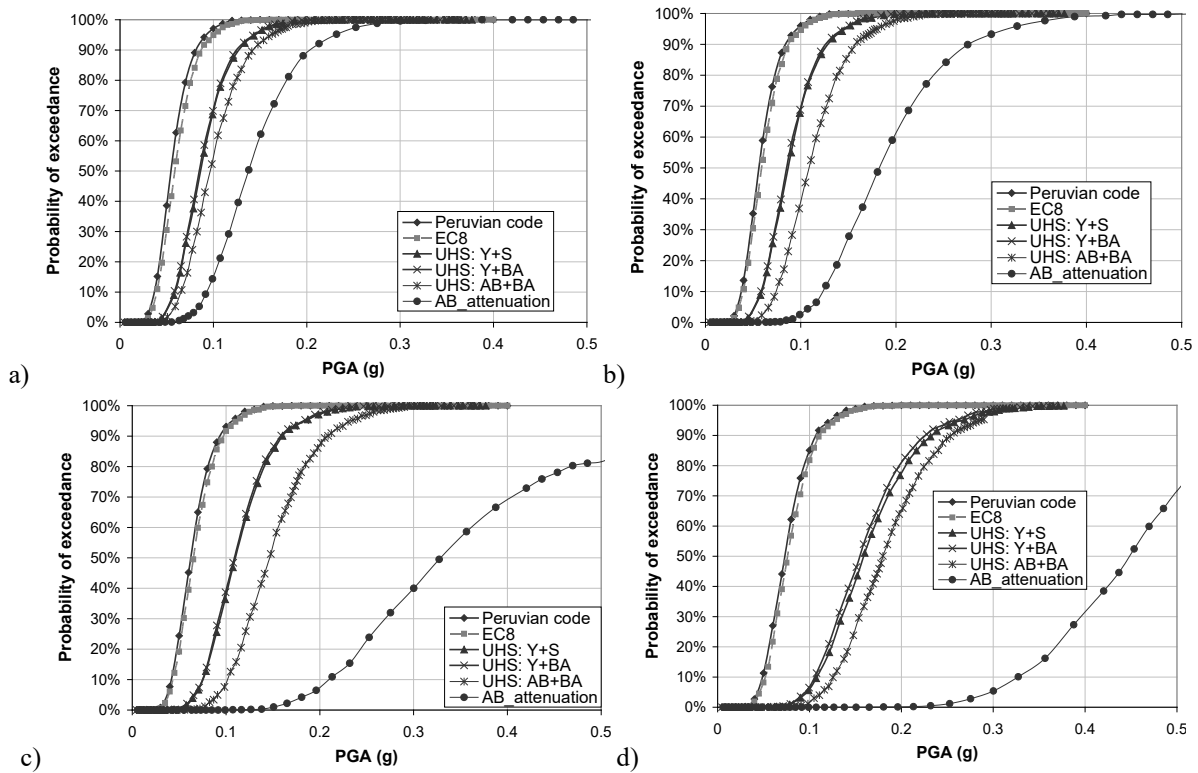


Figure 23. In-plane fragility curves in terms of PGA: (a) LS1, (b) LS2, (c) LS3, (d) LS4.

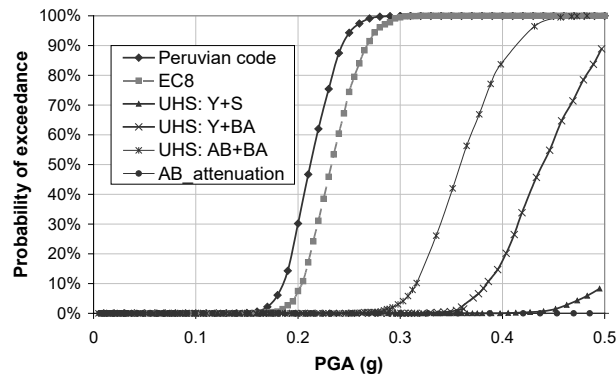


Figure 24. Out-of-plane fragility curves in terms of PGA and LS_{ii} .

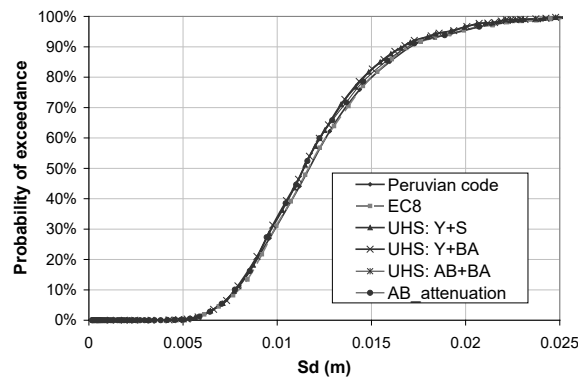


Figure 25. In-plane fragility curves in terms of mean limit state spectral displacement for LS4.

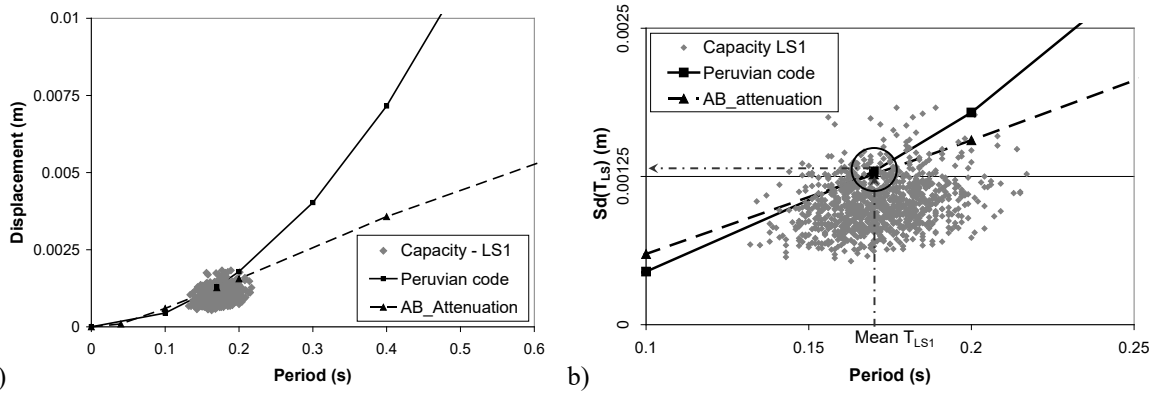


Figure 26. (a) Capacity versus demand comparison for the mean period of vibration TLS1, (b) detail of Figure 26a showing that the number of buildings with a displacement capacity lower than the demand is almost the same for both displacement spectra.

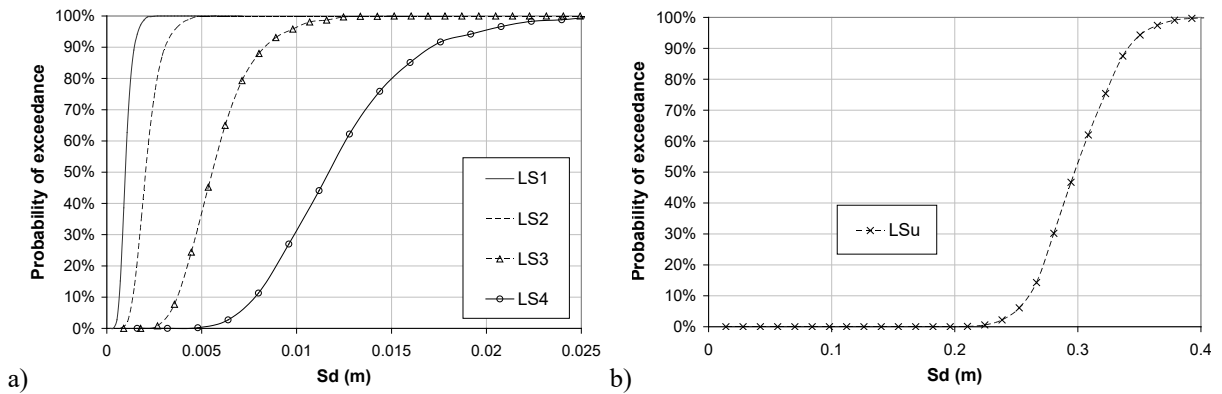


Figure 27. Fragility curves in terms of limit state spectral displacement: (a) in-plane, (b) out-of-plane.

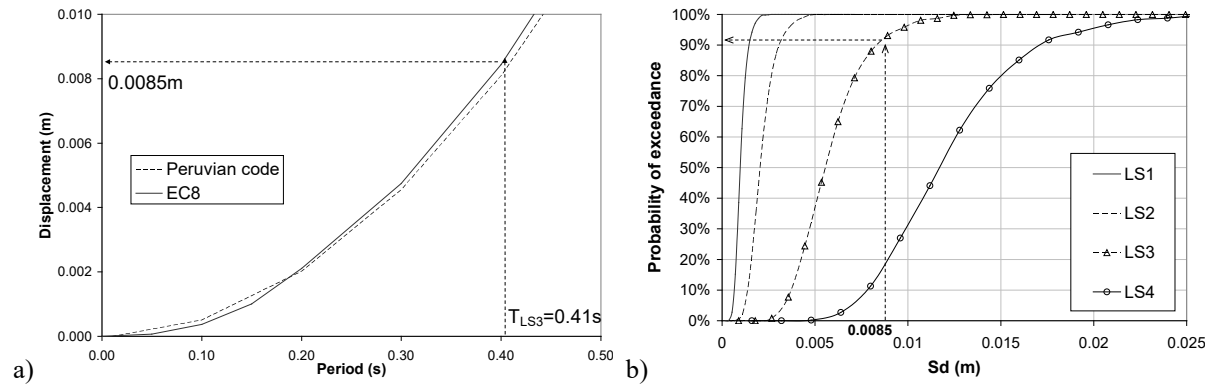


Figure 28. Procedure to evaluate the probability of exceedance of in-plane limit states: (a) spectral displacements for PGA = 0.1 g, (b) fragility curves for in-plane mechanism.

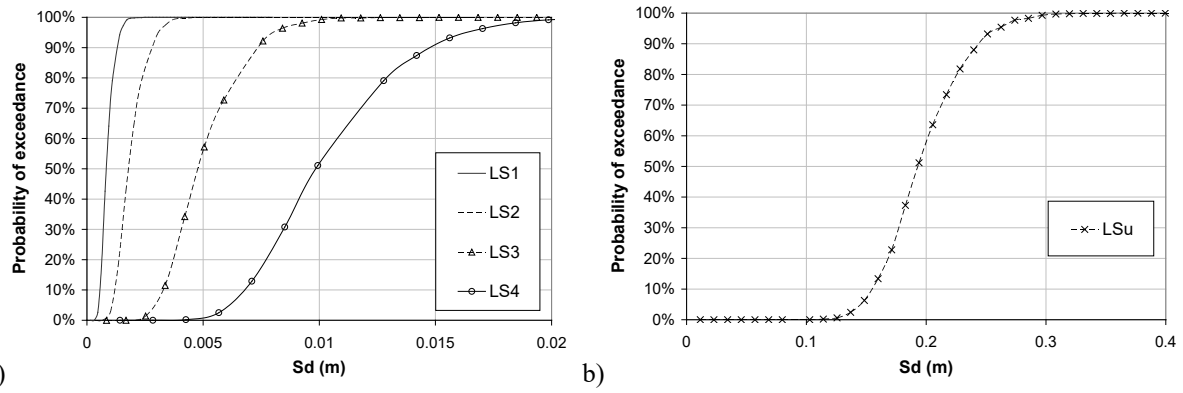


Figure 29. Fragility curves in terms of limit state spectral displacement for Pisco: (a) in-plane, (b) out-of-plane.

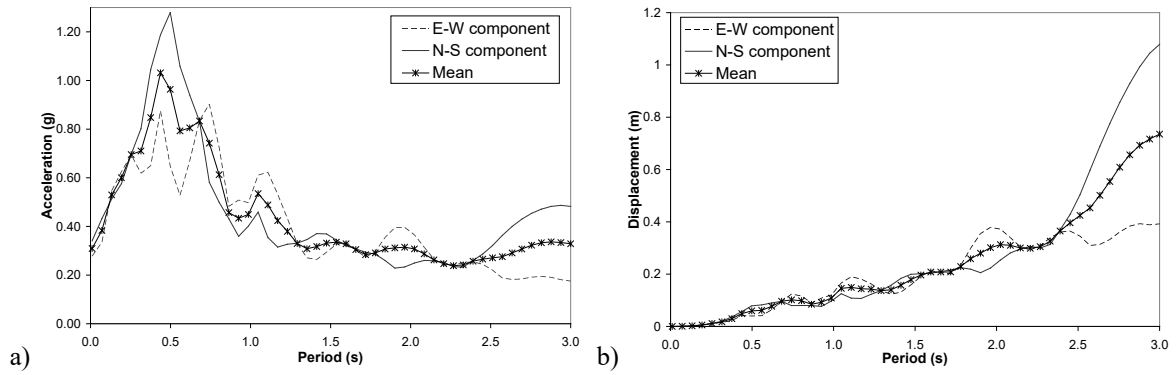


Figure 30. (a) ARS, (b) DRS obtained from Station ICA2.

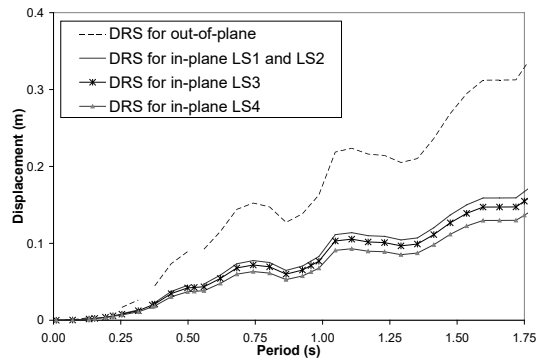


Figure 31. DRS shapes for each limit state, in-plane and out-of-plane.